

Automatic Vehicle Classification using Roadside LiDAR Data

Jianqing Wu¹, Hao Xu¹, Yichen Zheng¹, Yongsheng Zhang¹,
 Bin Lv², and Zong Tian¹

Transportation Research Record
 2019, Vol. 2673(6) 153–164
 © National Academy of Sciences:
 Transportation Research Board 2019
 Article reuse guidelines:
sagepub.com/journals-permissions
 DOI: 10.1177/0361198119843857
journals.sagepub.com/home/trr



Abstract

This research presented a new approach for vehicle classification using roadside LiDAR sensor. Six features (one feature, object height profile, contains 10 sub-features) extracted from the vehicle trajectories were applied to distinguish different classes of vehicles. The vehicle classification aims to assign the objects into ten different types defined by FHWA. A database containing 1,056 manually marked samples and their corresponding pictures was provided for analysis. Those samples were collected at different scenarios (roads and intersections, different speed limits, day and night, different distance to LiDAR, etc.). Naïve Bayes, K-nearest neighbor classification, random forest (RF), and support vector machine were applied for vehicle classification. The results showed that the performance of different methods varied by class. RF has the highest overall accuracy among those investigated methods. Some types were merged together to serve different types of users, which can also improve the accuracy of vehicle classification. The validation indicated that the distance between the object and the roadside LiDAR can influence the accuracy. This research also provided the distribution of the overall accuracy of RF along the distance to LiDAR. For the VLP-16 LiDAR, to achieve an accuracy of 91.98%, the distance between the object and LiDAR should be less than 30 ft. Users can set up the location of the roadside LiDAR based on their own requirements of the classification accuracy.

Vehicle classification data are valuable information for numerous transportation applications, such as road surveillance, traffic control, traffic safety, road planning, and pavement maintenance. For roadway design, it is appropriate to examine all vehicle types, establish general class groupings, and select vehicles of representative sizes within each class for design use (1). Vehicle classification data are also important for the development of automatic toll charging systems. Serving different purposes, there may be different vehicle classification schemes in operation. For example, in the Green Book *A Policy on Geometric Design of Highways and Streets* (2), four general classes of design vehicles were established; passenger cars, buses, trucks, and recreational vehicles. FHWA (3) divided the vehicles into 13 different types including motorcycles, passenger cars, buses, and ten types of trucks.

Various vehicle classification methods have been developed using different data collection methods. Those data collection methods include axle-based methods (pneumatic tube and piezoelectric detectors) (4), vehicle-sound-based methods (5), vehicle-length-based methods (loop detectors and blade) (6–10), video-based methods (11), and radar-based methods (12, 13). Each sensor technology has its own strengths and weaknesses

regarding costs, accuracy, performance, and ease of use (14). The Light Detection and Range (LiDAR, LIDAR, or laser) provides another data collection method for vehicle classification. LiDARs were firstly used in military applications to detect and identify vehicles by their range profiles (15). The LiDARs are now widely adopted for object perception and recognition in the autonomous vehicle field. Many studies have been conducted to use LiDAR-based methods for vehicle classification (14, 16–21). Lee and Coifman (14) used eight features representing vehicle shape extracted from side-fire LiDAR for vehicle classification. The algorithm can correctly classify more than 99.5% of non-occluded vehicles. Abdelbaki et al. (16) used laser intensity to classify vehicles in 2001. Later, Hussain and Moussa (17) developed a laser-intensity-based vehicle classification system using random neural network. The output of this system was one of five major classification categories: motorcycle, passenger car, pickup or van, single unit truck or bus, and

¹Department of Civil and Environmental Engineering, University of Nevada, Reno, NV

²Lanzhou Jiaotong University, Lanzhou, Gansu, China

Corresponding Author:

Address correspondence to Hao Xu: haox@unr.edu

tractor-trailer. The overall accuracy rate was about 92%. Nashashibi and Bargeton (18) developed a laser-based vehicle classification system based on different criteria: geometrical configuration, occlusion reasoning, sensor specifications, and tracking information. Harlow and Peng (19) used shape features extracted from laser sensor to classify different vehicles using a rule-based classifier. A total of 19 features including height, weight, and length were used to classify vehicles into 14 different classes. The overall correct classification rate was 92%. Sandhawalia et al. (20) focused on feature descriptors for supervised classification of laser scanner profiles. A 3D profile interpreted as a 2D image with depth values as pixel intensities was used for vehicle classification. The test results showed that the vehicle accuracy can be as high as 99.2%. Himmelsbach et al. (21) advocated the use of statistics of local point cloud properties, captured by histograms over point features for object feature extraction. A support vector machine (SVM) classifier was used to train the algorithm to classify different vehicle types. The results showed that this method can achieve an accuracy of 96.7%. Those abovementioned papers provide good references for LiDAR-based vehicle classification. However, there are some limitations in previous studies that can be further improved. First, there is a lack of studies using roadside LiDAR for vehicle classification. Most previous studies put efforts on airborne or on-board LiDAR (installed on moving vehicles). Only the study led by Coifman (14) focused on vehicle classification based on roadside LiDAR (work at a stationary location). The roadside LiDAR can provide vehicle classification data for road-based traffic or even lane-based traffic, while on-board LiDAR can only provide vehicle classification surrounding the moving vehicle. Second, most LiDARs used in previous studies were high-resolution LiDARs, which means the prices of those units were also high. It is not feasible to use high-cost LiDAR for vehicle classification considering the massive deployment requirements in the future. But if cost-effective LiDAR sensor is applied, it can only provide limited points for one scanned object, especially when the object is far away from the LiDAR.

This paper aims to classify vehicles using sparse points extracted from a cost-effective roadside 360° LiDAR sensor. In our research (22–27), we developed a LiDAR-enhanced roadside infrastructure serving connected vehicles (CV). Considering the abundant information that can be extracted from roadside LiDAR, the authors want to extend the application of roadside LiDAR to extract more useful information, such as vehicle classification. We tested the effectiveness of different methods on vehicle classification and recommended random forest (RF) for vehicle classification. This paper is structured as follows. First, the pre-processing of the roadside

LiDAR data is introduced. The feature selection is then documented. The different methods applied for vehicle classification are described and their performances compared. The last section summarizes the major conclusions and discussions for future research.

Data Pre-Processing of Roadside LiDAR

The selection of roadside LiDAR should consider the investment cost of the units. Therefore, only cost-effective LiDAR can be used for volume deployment. The price of different 360° LiDAR sensors was investigated. For example, the VLP-32C, which has 200 m of detection range is now priced at \$26,000 and the HDL-32E, which has 80–100 m of detection range is now priced at \$35,000. The price of the VLP-16 is \$2,000, which is more cost-effective than other investigated sensors. It should be noticed that the investigated price was based on the authors' best knowledge. There may be some deviation from the actual price. In this research, we selected the VLP-16 LiDAR manufactured by Velodyne for analysis. The major parameters of the VLP-16 are summarized in Table 1.

The LiDAR sensor can be temporarily installed on a tripod for pilot study or permanently installed on roadside structures for long-term data collection (23). Figure 1 shows two examples of roadside LiDARs installed by the authors for different purposes. The approximate height of the LiDAR location is 9 ft above the ground (23).

The pre-processing aims to extract vehicle point cloud for classification from the raw LiDAR data. The authors have developed a complete procedure to extract the trajectories of road users from the roadside LiDAR data. The framework of data processing is shown in Figure 2. The data processing (22–27) includes background filtering, lane identification, object clustering, and object tracking.

Table 1. Major Features of VLP-16

Horizontal field of view	360°
Rotation rate	5–20 Hz
Vertical field of view	30° ($\pm 15^\circ$)
Detection range	Up to 100 m
Channels	16
Angular resolution (vertical)	2°
Return models	Strongest, last, or dual return
Wave length	903 nm
Beam size at screen	9.5 mm \times 12.7 mm
Beam divergence	3 mrad
Power consumption	8 W (typical)
Accuracy	± 3 cm (typical)
Operation temperature	-10°C to +60°C
Storage temperature	-40°C to +105°C
Weight	803 g
Dimensions	103 mm diameter \times 72 mm height

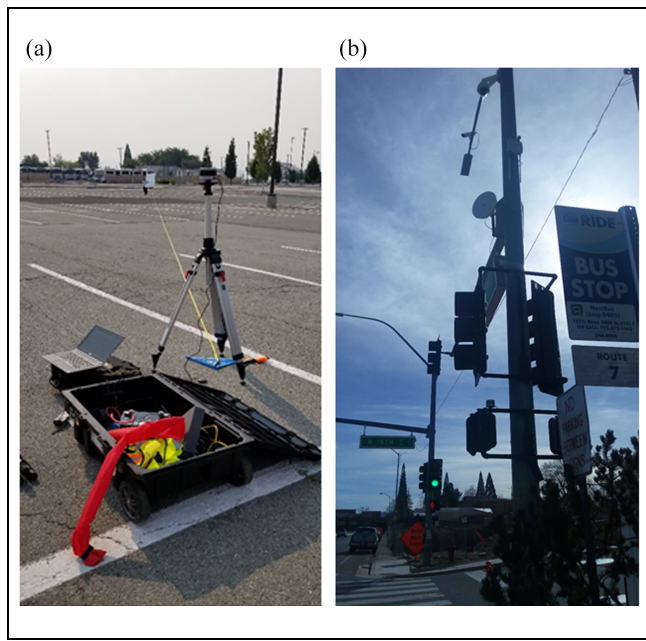


Figure 1. LiDAR installation: (a) portable roadside LiDAR and (b) permanently installed roadside LiDAR.

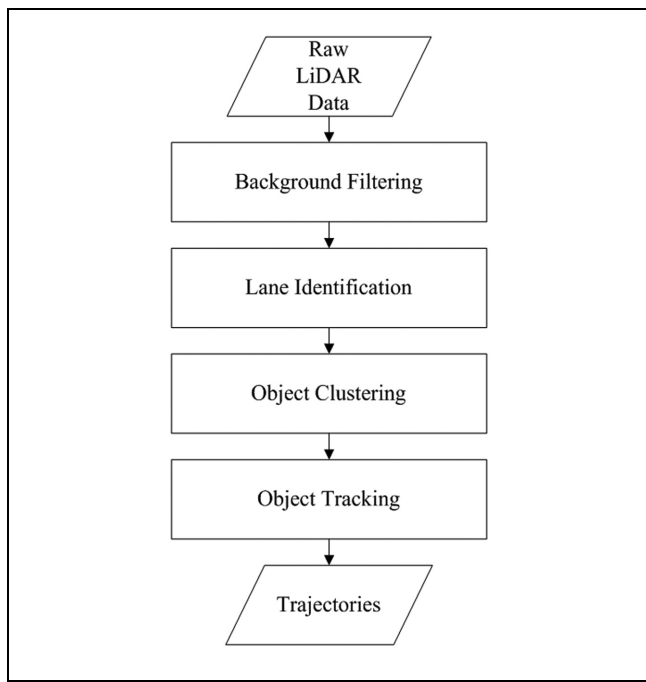


Figure 2. Flow chart of data pre-processing.

Background Filtering

Background points include buildings, trees, ground points, and so forth. Without excluding background points, it is difficult to cluster and identify the vehicle points correctly. An automatic 3D-density-statistics-background-filtering (3D-DSF) algorithm was developed by the authors (22). The idea of the 3D-DSF is briefly

summarized as follows. The algorithm firstly collects raw data in a period as initial input. The raw data are then aggregated into one 3D space based on their coordinates. The 3D space is then divided into multiple cubes for density statistics. Each cube can be identified as a background space or not. Compared with the group of background points and ground points, the number of moving vehicle points is fewer. Some cubes can be identified as background space by giving an appropriate threshold. A detailed automatic threshold learning was documented by the authors in another paper (24).

Lane Identification

Lane location is helpful to get lane-based traffic information. A lane identification algorithm, multi-rectified density-based spatial clustering of applications with noise (MCDBSCAN), developed by the authors (26) uses the vehicle trajectories in a time period to identify road boundaries. The idea of the MCDBSCAN is that after background filtering, the density of vehicle points should be much higher than other objects if multi frames are aggregated together. Similar with 3D-DSF, the whole space can be divided into small squares. Then by searching for the squares with high vehicle-points density, the squares representing road areas can be identified. The road boundary can be further extracted by searching the boundary of those squares representing road areas. The lane locations can be detected from the road boundaries with the width of the lanes.

Object Clustering

Points belonging to one object need to be clustered into one group. In a previous study by the authors (27), a revised density-based spatial clustering of applications with noise (DBSCAN) method was used for object clustering. The revised DBSCAN can have adaptive input parameters based on the different point density and distance to the LiDAR sensor.

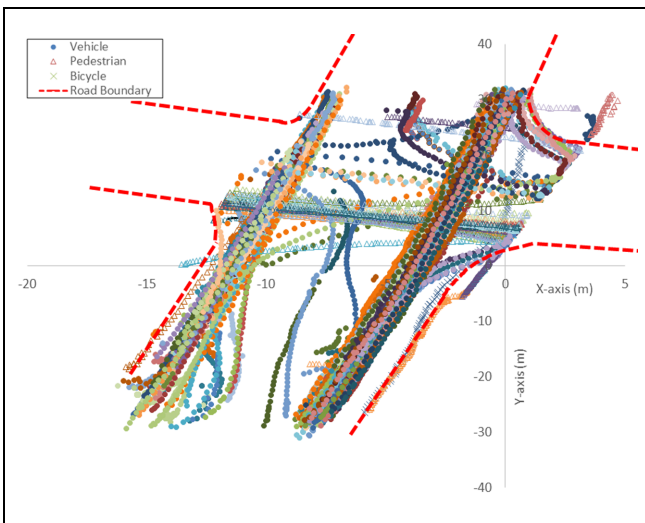
Object Tracking

Global nearest neighbor was applied to track the same vehicle in different frames (27). Two factors were considered for object association: distances between an object in a previous frame to all objects in the current frame, and the time difference between two considered frames. An object in the current frame was matched to an object in the previous frame if the distance between these two objects was the shortest among all the candidate objects within a certain time period. The candidate objects were selected by the area within the distance threshold. The pilot study (27) showed that the developed algorithm can detect the vehicle with a max distance of 30m from

Table 2. An Example of Information in the Trajectory

FrameID (timestamp)	ObjectID	LaneID	X	Y	Z	Speed (mph)
60	8	3	-8.24224	21.3304	1.55442	33.6877517
61	8	3	-8.51415	19.8953	1.51944	33.3386578
62	8	3	-8.72231	18.4309	1.44307	33.2724286
63	8	3	-8.94619	16.8296	1.3902	33.8102176
64	8	3	-9.17672	15.2833	1.33178	34.1008121
65	8	3	-9.39569	13.7902	1.37331	34.1263692
66	8	3	-9.63093	12.3663	1.40988	34.0523811
67	8	3	-9.85299	10.8807	1.23769	34.1553584
68	8	3	-10.0852	9.33633	1.12628	33.9090707
69	8	3	-10.1838	7.82723	1.08065	33.6604664
70	8	3	-10.4004	6.32561	1.03641	33.6968252
71	8	3	-10.6431	4.81187	0.978234	34.0996248
72	8	3	-10.914	3.35081	0.943973	34.0206101
73	8	3	-11.1481	1.91493	0.907171	33.5412528
74	8	3	-11.3602	0.488809	0.882104	33.2503926
75	8	3	-11.5625	-0.94298	0.870454	32.931783
76	8	3	-11.7352	-2.41331	0.446864	32.6917614
77	8	3	-11.9576	-3.85616	0.412941	32.5794066
78	8	3	-12.1542	-5.24951	0.463339	32.3673508

Note: ObjectID is a unique number representing the specific road user. LaneID is a number representing the location of traffic lane which the vehicle is using.

**Figure 3.** An example of trajectories of road users.

LiDAR sensor with high accuracy. Figure 3 shows an example of the trajectories of road users in 15 min collected at an intersection.

The data include XYZ position of points in each object, distance to LiDAR, tracking ID, frame number (timestamp), lane ID, velocity, and direction. An example was illustrated in Table 2. Though the main purpose of this paper is to classify vehicles into different types, the authors also put pedestrian and bicycle data into the database. This means the algorithm can also distinguish pedestrian, bicycle, and vehicle data.

Feature Selection

Appropriate features are very pivotal for vehicle classification algorithms. The features used for vehicle classification varied in previous studies. Table 3 shows the summary of different features used in previous studies. It was shown that the features representing vehicle shape were widely used in several studies. For LiDAR data, features representing vehicle shape can be extracted from the vehicle trajectories. Though intensity is also reported in the point cloud, the practice shows that it is unstable and changes between different objects subject to different reflecting strength and the angles between objects and LiDAR (24).

Inspired by previous work (9, 20, 24, 27), this paper used the following six features (in the bullets) for vehicle classification:

- Max length in the trajectory (ML). For each point cloud in the frames in the trajectory, the 3D points were firstly projected to XY plane (this means only XY coordinates were considered). Then a linear regression line can be easily generated to represent the length of the vehicle (L) (this is a rough value representing the length of the vehicle). The procedure was shown in Figure 4. Then ML can be easily generated using

$$ML = \max_{i=a:b} L_i \quad (1)$$

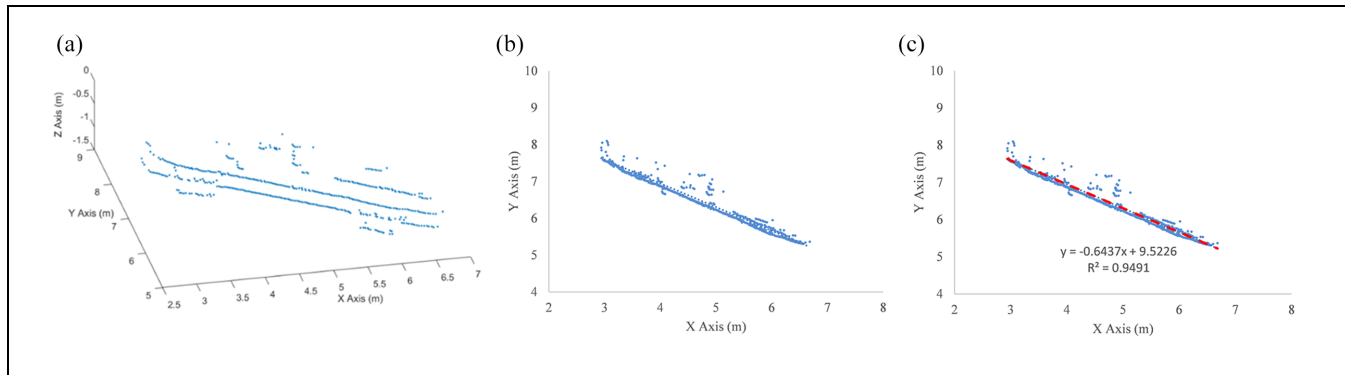


Figure 4. Vehicle length generation: (a) vehicle in 3D space, (b) vehicle in 2D space, and (c) length regression.

Table 3. Summary of Feature Selection in Previous Studies

Reference	Features
Nooralahiyah et al. (5)	Vehicle sound
Ki et al. (7)	Vehicle length
Zhang et al. (11)	Vehicle length
Urazghildiev et al. (12)	Vehicle height profile
Fang et al. (11)	Doppler signature
Abdelbaki et al. (15); Hussain and Moussa (16)	Intensity
Sandhawalia et al. (20)	The width of the profile (W), the length of the profile (L), the maximum height of the profile, number of units, the maximum height of the first unit.
Oh and Ritchie (9)	Vehicle length, maximum magnitude of inductance change, standard deviation, shape parameter, degree of symmetry, and so forth
Jeng and Ritchie (10)	Piecewise slope rate (PSR) features
Harlow and Peng (19)	A total of 19 features including height, weight and length
Oh et al. (8)	Vehicle specific feature vectors
Himmelsbach et al. (21)	Intensity, lalonde features, and anguelov feature
Lee and Coifman (14)	Vehicle length, height, detection of middle drop, vehicle height at middle drop, front vehicle height, front vehicle length, rear vehicle height and rear vehicle length
Zhao et al. (27)	Number of points, distance to LiDAR, spatial distribution direction

where ML is the max length of object in the trajectory; i is the frame ID; a is the begin tracking frame ID; b is the end tracking frame ID; L_i is the object length in frame i .

- Max height in the trajectory (MH). For each frame, the 3D points were projected to the plane created by the length regression line and Z-axis, as seen in Figure 4. The object height can be estimated using the difference between max Z-value and min Z-value. MH can be calculated using

$$ML = \max_{i=a:b} (\text{MaxZ}_i - \text{MinZ}_i) \quad (2)$$

- where MH is the max height of object in the trajectory; i is the frame ID; a is the begin tracking frame ID; b is the end tracking frame ID; MaxZ_i is the max Z value in frame i . MinZ_i is the min Z value in frame i . Figure 5 illustrates the MH extraction.
- Nearest distance from object points to LiDAR (D).
- Number of points in the frame with max length (N).
- Difference between length and height (DLH) $DLH = ML - MH$. DLH can be very useful to distinguish vehicles and pedestrians. It is found that for vehicle, ML is usually longer than MH ; for pedestrian, ML is usually smaller than MH .
- Object height profile (OHP). This feature contains the detailed vehicle shape information along the vehicle length. For each object, it can be divided into n small equal columns covering the max z-value and min z-value along the vehicle length direction. In each column, the max height can be calculated. Then OHP is a $1 \times n$ matrix that contains n sub-features. Each sub-feature is the max height in the column. The sequence of the sub-

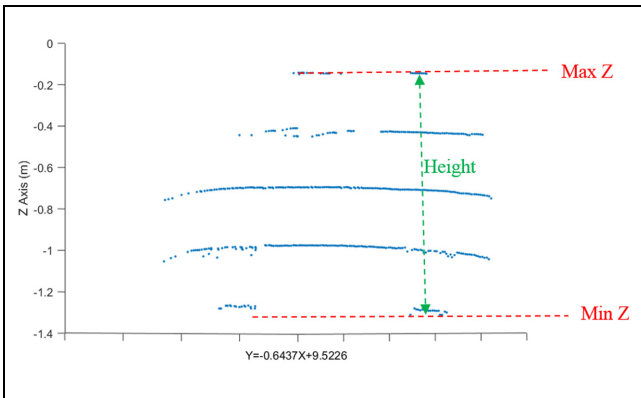


Figure 5. Object height estimation.

feature is from back to front of the vehicle. Then OHP can be obtained by

$$\text{OHP} = [\text{MaxH}_1 \quad \dots \quad \text{MaxH}_n] \quad (3)$$

- where n is the number of columns and MaxH is the max height in the column. In this paper, n is selected as 10 based on the practice (too few sub-features may not provide the obvious difference for different vehicle types and too many sub-features can generate big variance between adjacent sub-features). Different types of objects have different OHP, as shown in Figure 6. Different moving directions can influence the sequence of the sub-feature. For example, if we assume vehicles pass the roadside LiDAR from left to right, for the moving direction close to the LiDAR, the leftmost column should be considered as OHP_1 . If the vehicle uses the other opposite direction, the rightmost column should be considered as OHP_{10} .

A database containing 1,056 samples was built for vehicle classification. The data were collected at three

different sites. The summary information of the data collection is shown in Table 4.

The samples included the data collected at different scenarios (roads and intersections, different speed limits, day and night, etc.). The samples were manually marked based on the FHWA vehicle classification standard (3). Among the 1,056 samples, 724 of them were selected as the training set and the other 332 samples were used for testing. To overcome the overfitting issue, in the training dataset, 483 samples were used for training and 241 samples were used for validation. To further reduce the variability, cross validation was used to partition the training set and validation set. The cross validation was automatically performed using the “seed” function in R. The detailed types are documented in Table 5. It is shown that the number of different classes is imbalanced. (It is normal knowledge that passenger cars have the highest proportion among different classes.)

Vehicle Classification Methods

The reported methods used for vehicle classification in previous studies included Naïve Bayes (NB) (28–30), K-nearest neighbor classification (KNN) (31), decision (classification) tree (32), support vector machine (SVM) (21, 33, and 34), and artificial neural network (ANN) (5, 7, 35–37). This section briefly introduces these methods and applies some of them for vehicle classification.

Brief Introduction about Different Methods

NB. NB methods are a set of supervised learning algorithms based on applying Bayes’ theorem. NB methods assume that the presence of one feature in a class is conditionally independent to the presence of all other features (28). Given a class variable y and a dependent feature vector x_1 through i_n , a naïve Bayes model follows the classification rule

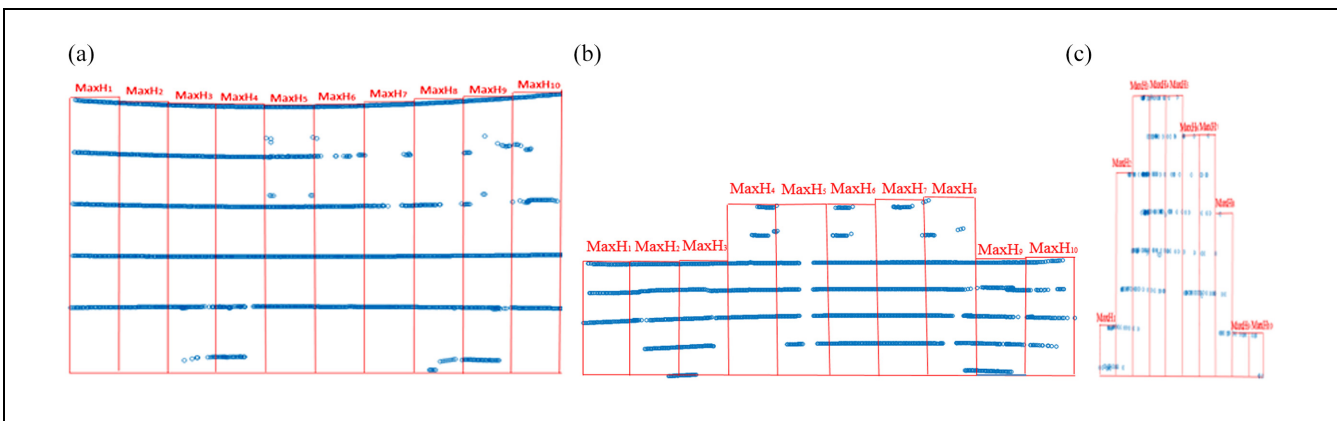


Figure 6. Object height profile (OHP): (a) bus, (b) pickup truck, and (c) pedestrian.

Table 4. Data Collection Sites

Location	Road/intersection	AADT	Speed limit (mph)	Data collection time	Night time covered
I-80 freeway in Elko	Road segment	11,800	80	Morning peak hours: high vehicle volume	No
N Virginia St at 15th St	Intersection	11,000	35	Morning peak hours and non-peak hours: high pedestrian volume	No
N Virginia St at 10th St	Intersection	1,500	25	Afternoon peak hours and non-peak hours	Yes

Note: AADT = annual average daily traffic.

Table 5. Classes of Objects

Group	Training set	Testing set	Code	Note
Pedestrians and skateboarder	152	22	0	Code defined by the authors
Bicycle	12	3	-1	Code defined by the authors
Motorcycle	26	14	1	Code defined by FHWA
Passenger car	199	150	2	Code defined by FHWA
Four-tire, single unit	105	69	3	Code defined by FHWA
Bus	69	20	4	Code defined by FHWA
Two-axle, six-tire, single-unit truck	33	17	5	Code defined by FHWA
Three-axle, single-unit truck	11	4	6	Code defined by FHWA
Four or fewer axle, single-trailer truck	3	0	8	Code defined by FHWA
Five-axle, single-trailer truck	124	17	9	Code defined by FHWA

Note: The actual classes of vehicles defined by FHWA (3) are more than the lists in Table 5. The other types were not included since they were not captured during the data collection.

$$P(y|x_1, \dots, x_n) \propto \prod_{i=1}^n P(x_i|y) \quad (4)$$

NB works better for categorical variables than for numeric features.

KNN. KNN is an instance-based classification method. An object is classified by a majority vote of its neighbors, with the object being assigned to the class most common among its K-nearest neighbors (31). The KNN does not make any assumptions on the underlying data distribution, which means the model structure is determined from the data. This also means that the KNN is sensitive to the irrelevant features and the scales of the data.

Decision Tree. Decision tree is a type of supervised learning algorithm that can be used for both regression and classification. A single decision tree may be prone to a noise, but aggregate of many decision trees, such as RF, can reduce the effect of noise, giving more accurate results. RF provides an improvement over bagged trees by a small tweak that decorrelates the trees. RF can balance errors in datasets where the classes are imbalanced and works well for massive datasets with large dimensionality.

SVM. SVM is also a supervised learning method which is defined by a separating hyperplane. This algorithm can output an optimal hyperplane by maximizing the margin between the classes' closest points using the labeled training data (33). The SVM may be very sensitive to the proper choice of kernel parameters. The SVM was originally developed for binary classification. However, now SVM can be also used for multi-class classification by fitting all binary sub-classifiers and finding the correct class by a voting mechanism (34).

ANN. The ANN is a system that uses the artificial neurons to build the connection between the input features and classification results. An ANN can have multiple hidden layers between the input and output data. Typically, the more layers, the more computational time required. One widely used ANN is backpropagation artificial neural network (BP-ANN) (27). The input data is fed into the input layer. Then, the activity of each hidden layer is determined by the inputs and the weights that connect the input layer and hidden layer. A similar process takes place between the hidden layer and output layer. The transmission from one neuron in one layer to another neuron in the next layer is independent. The output layer produces the estimated outcomes. The comparison information (error) between target outputs and estimated outputs is given back to the input layer as a

Table 6. CCR of Different Methods

Class	Class code	Test samples	CCR (%)			
			NB	RF ^a	SVM ^b	KNN ^c
Four or fewer axle, single-trailer truck	8	0	NA	NA	NA	NA
Two-axle, six-tire, single-unit truck	5	17	31.3	43.8	12.5	31.3
Bus	4	20	95.0	100.0	0.5	100.0
Bicycle	-1	3	33.3	0.0	0.0	0.0
Five-axle, single-trailer truck	9	17	0.0	100.0	100.0	94.1
Motorcycle	1	14	7.1	0.0	0.0	0.0
Three-axle, single-unit truck	6	4	100.0	0.0	0.0	0.0
Four-tire, single unit	3	69	53.6	69.9	55.4	47.0
Passenger car	2	150	64.4	84.4	66.7	68.1
Pedestrians and skateboarder	0	22	72.7	100.0	95.5	90.9
Overall accuracy			56.7	75.8	58.6	61.2

Note: CCR = correct classification rate; NB = Naïve Bayes; RF = random forest; SVM = support vector machine; KNN = K-nearest neighbor classification; NA = not applicable.

^aThe number of trees used in the RF is 500.

^bRadial basis function kernel is used for optimization in SVM.

^ck = 19, which is selected by the algorithm automatically based on the accuracy.

guide to adjust the weights in the next training round. Through this iteration process, the neural network gradually learns the inner relationship between input and output by adjusting the weights for each neuron in each layer to reach the best accuracy. When the minimal error is reached, or the number of iterations is beyond the pre-defined value, the training process is terminated with fixed weights. However, the BP-ANN suffers from two major drawbacks: low convergence rate and instability. The probabilistic neural network (PNN) is an efficient algorithm widely used for vehicle classification. The PNN uses Parzen estimators to construct the probability density functions (PDFs) of the different classes based on Bayes' rule (35). The PNN consists of four layers: input layer, pattern layer, summation layer, and output layer. The PNN operates entirely in parallel, unlike many other neural networks, without the need for feedback from individual neurons to the preceding layer of neurons (36). The only parameter to be calibrated in training is the smoothing parameter σ , which can be readily determined experimentally (35).

Training and Testing

The previous study suggested that for classification problems there is not a clear best choice when it comes to selection of an appropriate classifier (38). In this research, we used four different methods: NB, KNN, RF, and SVM. The performance of different methods was compared. The correct classification rate (CCR) represents the percentage of total vehicles that was correctly classified and is used to summarize the results (38). The class specific CCR during the testing procedure was calculated in Table 6.

The performance of different methods varies by class. The NB can identify three-axle single-unit trucks with an accuracy of 100% but could not distinguish five-axle single-trailer trucks correctly (an accuracy of zero). RF, SVM, and KNN can identify five-axle single-trailer trucks with an accuracy of 100% but could not distinguish three-axle single-unit trucks from the testing database. The RF can provide the highest accuracy for identify the group-passenger car with the largest sample size. The result also showed that the CCR of motorcycle and bicycle using the four methods is low. By checking the confusion matrix, it was found that typical misclassification type was 1→2 (misclassification among bicycle, motorcycle, and pedestrian). For misclassification between bicycle and motorcycle, it is also a challenge to use the shape information to distinguish them. The pedestrian may have different shapes considering the movement of the body, as shown in Figure 7. The pedestrian crossing the intersection in Figure 7 has relatively longer distance between two legs compared with the worker standing near the LiDAR. By checking the pictures, it was also found that the distance between two legs was longer if the pedestrian was running and the pedestrian may be some other arbitrary shape if he or she was carrying some larger object. The uncertain shape of the pedestrian increased the risk of misclassification.

It was also found that another misclassified type was 2→3 (wrong classification between passenger cars and four-tire single-unit). By manually checking the picture, it was shown that SUV (belonging to passenger car) and pickup truck (belonging to four-tire single-unit) might have fairly similar shape. Figure 8 shows an example. In Figure 8, it is easy to misclass even through manual observation.

Some other common misclassification types included

Table 7. CCR after Merging Group

Class	Class code	Test samples	CCR (%)			
			NB	RF ^a	SVM ^b	KNN ^c
Bus	4	20	95.0	100.0	45.0	100.0
Five-axle, single-trailer truck	9	17	0.0	94.1	0.0	100.0
Bicycle; motorcycle	-11	17	5.9	5.9	5.9	5.9
Three-axle, single-unit truck	6	4	100.0	0.0	0.0	0.0
Passenger car; four-tire, single unit; two-axle, six-tire, single-unit truck	235	236	91.1	93.2	94.5	90.2
Pedestrians and skateboarder	0	22	72.7	100.0	86.4	86.4
Overall accuracy			80.9	88.9	80.0	85.7

Note: CCR = correct classification rate; NB = Naïve Bayes; RF = random forest; SVM = support vector machine; KNN = K-nearest neighbor classification.

^aThe number of trees used in the RF is 400.

^bRadial basis function kernel is used for optimization in SVM.

^ck = 15, which is selected by the algorithm automatically based on the accuracy.



Figure 7. Different shapes of pedestrians.

- 3→5 (misclassification between four-tire single-unit and two-axle six-tire single-unit since the difference of tires was difficult to be captured by the roadside LiDAR, especially when the vehicle was far away from the LiDAR).
- 2→5 (usually occurred between SUV and two-axle six-tire single-unit).
- 3→9 (misclassification between four-tire single-unit and truck). This usually referred to the

situation that the pickup with a trailer was misclassified to the other type, as shown in Figure 9. The shape of the marked vehicle in Figure 9 is quite different from the shape of a common pickup.

Optional Classes Division

For some applications, such as auto-toll charging or simple traffic volume count, it may be not necessary to distinguish vehicles into such detailed types. Therefore, some types of vehicles in Table 3 can be merged together. Considering the high similarity between SUV, pickup and two-axle six-tire single-unit, Type “2,” “3,” and “5” can be merged together (we use Type “235” to represent the merged group). Bicycle and motorcycle also had the similar shape in LiDAR data, which was also merged in this part. Type “-11” was used to represent the merged group of Type “-1,” bicycle and Type “1,” motorcycle. Table 7 summarizes the CCR of different methods based on testing database after merging classes.

The RF still had the highest overall accuracy among the four investigated methods after merging the groups.

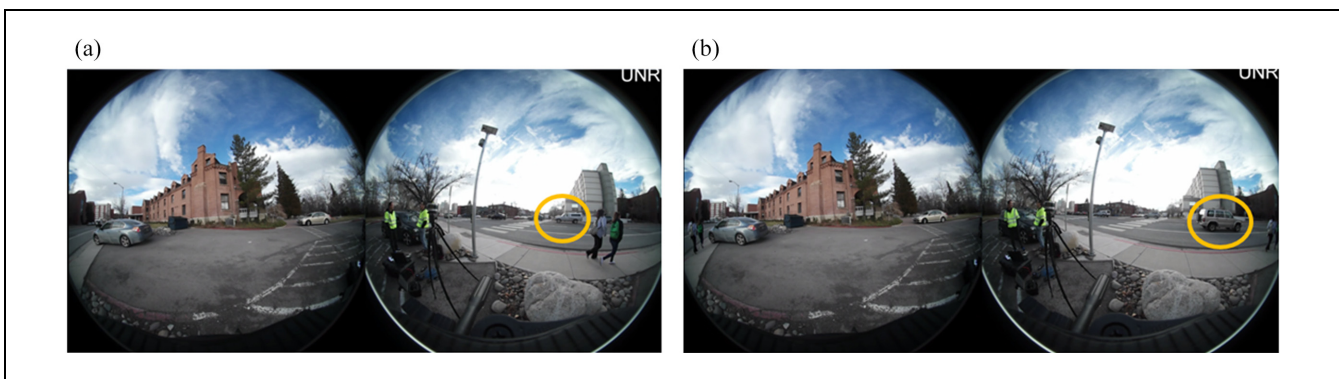


Figure 8. Misclassification between pickup and SUV: (a) pickup truck and (b) SUV.



Figure 9. Pickup with a trailer.

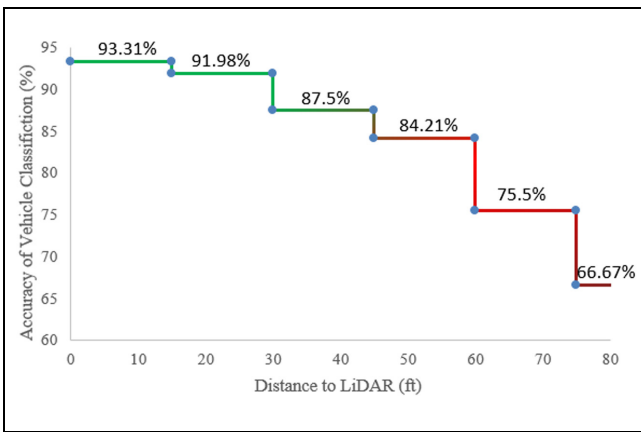


Figure 10. Accuracy distribution with distance to LiDAR.

The accuracy of Type “235” in Table 7 increased a lot compared with the separate accuracy of Type “2,” “3,” and “5” in Table 6. Table 7 also shows that the accuracy of the new Type “–11” is still low (5.9% for all four methods) after group integration. By checking the confusion matrix, it was found that a common error was the misclassification between “0” and “–11.” If the bicycle/motorcycle data are excluded from the training and testing dataset, then the accuracy of RF will be 92.6%. If the different types of trucks are merged together, the accuracy of RF can be further improved.

By checking the LiDAR data, it was found that the wrong classification between “0” and “–11” usually happened when the object (pedestrian/bicycle/motorcycle) was far away from the LiDAR. This indicated that the distance of the object to LiDAR might impact the performance of RF. Figure 10 demonstrates the distribution of the accuracy of RF for vehicle classification with different distances using the dataset after merging classes.

It is shown that the accuracy of vehicle classification decreases with the increasing distance to LiDAR. For the VLP-16 roadside LiDAR, to achieve an accuracy of 91.98%, the distance of the object to LiDAR should be less than 30 ft, whereas to achieve an accuracy of

84.21%, the distance of the object only needs to be no further than 60 ft to LiDAR. Users can use the distribution of accuracy to better select the location for LiDAR deployment.

Conclusion and Discussion

This paper presents a systematic procedure of vehicle classification using roadside LiDAR data. The shape features extracted from the trajectories of the object are used to distinguish different classes. This research built a comprehensive database including point clouds, manually marked objects, and corresponding pictures, which is open to all researchers for vehicle classification methods development or improvement. Different vehicle classification methods were investigated using the database built in this study. RF has the highest overall accuracy among the investigated methods. The testing results also indicated that the distance between objects and roadside LiDAR can influence the performance of vehicle classification.

The imbalanced classes (the number of objects in different classes is not the same) and the small sizes of some vehicle types may influence the accuracy of vehicle classification. More data samples are expected to be collected to further evaluate the performance of the proposed method in future studies. The validation showed that it was difficult to distinguish bicycle, motorcycle, and pedestrian using the current method. The speed of objects may be involved to distinguish motorcycle/bicycle/pedestrian in future studies (normally motorcycle speed > bicycle speed > pedestrian speed). The classification between SUV, pickup trucks, and two-axle six-tire single-unit is a challenge. The test results showed that grouping those classes can improve the accuracy of vehicle classification. The previous study (39) showed that the performance of the LiDAR degraded by heavy fog and blowing snow where visibility ≤ 20 ft (6 m). Therefore, this proposed method did not work for vehicle classification under extreme weather conditions.

There are some other methods (such as PNN) which are not examined in this paper. The previous study indicated that the combination of multiple classifiers may increase the prediction (30, 38). It is expected that the other methods such as PNN or the combination of different methods will be tested to further improve the accuracy of vehicle classification.

Acknowledgments

The work described in the paper was supported by Natural Science Foundation of China (No.61463026, 61463027), Foundation of A Hundred Youth Talents Training Program of Lanzhou Jiaotong University.

Author Contributions

The authors confirm contribution to the paper as follows: study conception and design: Jianqing Wu, Hao Xu, Yichen Zheng, Yongsheng Zhang, Bin Lv, Zong Tian; data processing: Jianqing Wu, Yongsheng Zhang, Bin Lv; analysis and interpretation of results: Jianqing Wu, Hao Xu, Yichen Zheng; draft manuscript preparation: Jianqing Wu, Yichen Zheng, Bin Lv. All authors reviewed the results and approved the final version of the manuscript.

References

1. *Policy on Geometric Design of Highways and Streets*. American Association of State Highway and Transportation Officials, Washington, D.C., 2011.
2. Hancock, M. W., and B. Wright. *A Policy on Geometric Design of Highways and Streets*. The American Association of State Highway and Transportation Officials, 2013.
3. *Traffic Monitoring Guide*. FHWA, 2016.
4. Martin, P. T., Y. Feng, and X. Wang. *Detector Technology Evaluation*. No. MPC Report No. 03-154. Mountain-Plains Consortium, Fargo, N.Dak., 2013.
5. Nooralahiyani, A. Y., M. Dougherty, D. McKeown, and H. R. Kirby. A Field Trial of Acoustic Signature Analysis for Vehicle Classification. *Transportation Research Part C: Emerging Technologies*, Vol. 5, No. 3–4, 1997, pp. 165–177.
6. Meta, S., and M. G. Cinsdikici. Vehicle-Classification Algorithm Based on Component Analysis for Single-Loop Inductive Detector. *IEEE Transactions on Vehicular Technology*, Vol. 59, No. 6, 2010, pp. 2795–2805.
7. Ki, Y. K., and D. K. Baik. Vehicle-Classification Algorithm for Single-Loop Detectors Using Neural Networks. *IEEE Transactions on Vehicular Technology*, Vol. 55, No. 6, 2006, pp. 1704–1711.
8. Oh, S., S. Ritchie, and C. Oh. Real-Time Traffic Measurement from Single Loop Inductive Signatures. *Transportation Research Record: Journal of the Transportation Research Board*, 2012. 1804: 98–106.
9. Oh, C., and S. G. Ritchie. Recognizing Vehicle Classification Information from Blade Sensor Signature. *Pattern Recognition Letters*, Vol. 28, No. 9, 2007, pp. 1041–1049.
10. Jeng, S. T., and S. Ritchie. Real-Time Vehicle Classification Using Inductive Loop Signature Data. *Transportation Research Record: Journal of the Transportation Research Board*, 2008. 2086: 8–22.
11. Zhang, G., R. Avery, and Y. Wang. Video-Based Vehicle Detection and Classification System for Real-Time Traffic Data Collection Using Uncalibrated Video Cameras. *Transportation Research Record: Journal of the Transportation Research Board*, 2007. 1993: 138–147.
12. Urazghildiiev, I., R. Ragnarsson, P. Ridderstrom, A. Rydberg, E. Ojefors, K. Wallin, and G. Lofqvist. Vehicle Classification Based on the Radar Measurement of Height Profiles. *IEEE Transactions on Intelligent Transportation Systems*, Vol. 8, No. 2, 2007, pp. 245–253.
13. Fang, J., H. Meng, H. Zhang, and X. Wang. A Low-Cost Vehicle Detection and Classification System Based on Unmodulated Continuous-Wave Radar. *Proc., IEEE Conference on Intelligent Transportation Systems Conference*, Seattle, IEEE, New York, 2007.
14. Lee, H., and B. Coifman. Side-Fire Lidar-Based Vehicle Classification. *Transportation Research Record: Journal of the Transportation Research Board*, 2012. 2308: 173–183.
15. Sun, Y., H. Xu, J. Wu, J. Zheng, and K. M. Dietrich. 3-D Data Processing to Extract Vehicle Trajectories from Roadside LiDAR Data. *Transportation Research Record: Journal of the Transportation Research Board*, Vol. 2627, No. 45, 2018, pp. 14–12.
16. Abdelbaki, H. M., K. Hussain, and E. Gelenbe. A Laser Intensity Image Based Automatic Vehicle Classification System. *Proc., IEEE Conference on Intelligent Transportation Systems Conference*, Oakland, IEEE, New York, 2001.
17. Hussain, K. F., and G. S. Moussa. Laser intensity vehicle classification system based on random neural network. Presented at 43rd Annual Meeting of the Transportation Research Board, Washington, D.C., 2005.
18. Nashashibi, F., and A. Bargeron. Laser-Based Vehicles Tracking and Classification Using Occlusion Reasoning and Confidence Estimation. *Proc., IEEE Conference on Intelligent Vehicles Symposium*, Eindhoven, Netherlands, IEEE, New York, 2008.
19. Harlow, C., and S. Peng. Automatic Vehicle Classification System with Range Sensors. *Transportation Research Part C: Emerging Technologies*, Vol. 9, No. 4, 2001, pp. 231–247.
20. Sandhawalia, H., J. A. Rodriguez-Serrano, H. Poirier, and G. Csurka. Vehicle Type Classification from Laser Scanner Profiles: A Benchmark of Feature Descriptors. *Proc., IEEE Conference on Intelligent Transportation Systems*, Hague, Netherlands, IEEE, New York, 2013.
21. Himmelsbach, M., T. Luettel, and H. J. Wuensche. Real-Time Object Classification in 3D Point Clouds Using Point Feature Histograms. *Proc., IEEE/RSJ International Conference on Intelligent Robots and Systems*, St. Louis, IEEE, New York, 2009.
22. Wu, J., H. Xu, and J. Zheng. Automatic Background Filtering and Lane Identification with Roadside LiDAR Data. *Proc., IEEE 20th International Conference on Intelligent Transportation*, Yokohama, Japan, IEEE, New York, 2017.
23. Wu, J., and H. Xu. An Automatic Procedure for Vehicle Tracking with a Roadside LiDAR Sensor. Presented at 97th Annual Meeting of the Transportation Research Board, Washington, D.C., 2018.
24. Wu, J., H. Xu, Y. Sun, J. Zheng, and R. Yue. Automatic Background Filtering Method for Roadside Lidar Data. *Transportation Research Record: Journal of the Transportation Research Board*, Vol. 2627, No. 45, 2018, pp. 106–114.
25. Zheng, Y., H. Xu, Z. Tian, and J. Wu. Design and Implementation of the DSRC Bluetooth Communication and Mobile Application with LiDAR Sensor. Presented at 97th Annual Meeting of the Transportation Research Board, Washington, D.C., 2018.
26. Wu, J., H. Xu, and J. Zhao. Automatic Lane Identification Using the Roadside LiDAR Sensors. *IEEE Intelligent Transportation Systems Magazine*, in press, 2018.

27. Zhao, J., H. Xu, D. Wu, and H. Liu. An Artificial Neural Network to Identify Pedestrians and Vehicles from Roadside LiDAR Data. Presented at 97th Annual Meeting of the Transportation Research Board, Washington, D.C., 2018.
28. Premeida, C., O. Ludwig, and U. Nunes. LIDAR and Vision-Based Pedestrian Detection System. *Journal of Field Robotics*, Vol. 26, No. 9, 2009, pp. 696–711.
29. Hernandez, S. V., A. Tok, and S. G. Ritchie. Integration of Weigh-in-Motion (WIM) and Inductive Signature Data for Truck Body Classification. *Transportation Research Part C: Emerging Technologies*, Vol. 68, 2016, pp. 1–21.
30. Hernandez, S., A. Tok, and S. G. Ritchie. Multiple-Classifier Systems for Truck Body Classification at WIM Sites with Inductive Signature Data. Presented at 94th Annual Meeting of the Transportation Research Board, Washington, D.C., 2015.
31. Tan, M., B. Wang, Z. Wu, J. Wang, and G. Pan. Weakly Supervised Metric Learning for Traffic Sign Recognition in a LIDAR-Equipped Vehicle. *IEEE Transactions on Intelligent Transportation Systems*, Vol. 17, No. 5, 2016, pp. 1415–1427.
32. Joshi, N., B. George, and L. Vanajakshi. Application of Random Forest Algorithm to Classify Vehicles Detected by a Multiple Inductive Loop System. *Proc., IEEE Conference on Intelligent Transportation Systems*, Anchorage, Alaska, IEEE, New York, 2012, pp. 491–495.
33. Chen, Z., N. Pears, M. Freeman, and J. Austin. Road Vehicle Classification Using Support Vector Machines. *Proc., IEEE Conference on Intelligent Computing and Intelligent Systems*, Shanghai, China, 2009, pp. 214–218.
34. Zhou, J., D. Gao, and D. Zhang. Moving Vehicle Detection for Automatic Traffic Monitoring. *IEEE Transactions on Vehicular Technology*, Vol. 56, No. 1, 2007, pp. 51–59.
35. Abdulhai, B., and S. G. Ritchie. Enhancing the Universality and Transferability of Freeway Incident Detection Using a Bayesian-Based Neural Network. *Transportation Research Part C: Emerging Technologies*, Vol. 7, No. 5, 1999, pp. 261–280.
36. Oh, C., J. S. Oh, and S. G. Ritchie. Real-Time Hazardous Traffic Condition Warning System: Framework and Evaluation. *IEEE Transactions on Intelligent Transportation Systems*, Vol. 6, No. 3, 2005, pp. 265–272.
37. Oh, C., Y. S. Kang, Y. Youn, and A. Konosu. Development of Probabilistic Pedestrian Fatality Model for Characterizing Pedestrian-Vehicle Collisions. *International Journal of Automotive Technology*, Vol. 9, No. 2, 2008, pp. 191–196.
38. Hernandez, S. V., A. Tok, and S. G. Ritchie. Integration of Weigh-in-Motion (WIM) and Inductive Signature Data for Truck Body Classification. *Transportation Research Part C: Emerging Technologies*, Vol. 68, 2016, pp. 1–21.
39. Klein, L. A. *ITS Sensors and Architectures for Traffic Management and Connected Vehicles*. Taylor and Francis, Boca Raton, Fla., 2017.

The Standing Committee on Highway Traffic Monitoring (ABJ35) peer-reviewed this paper (19-00874).